

RECEIVED: February 6, 2019

REVISED: April 29, 2019

ACCEPTED: May 16, 2019

PUBLISHED: May 24, 2019

LHC constraints on a $B - L$ gauge model using CONTUR

S. Amrith, J.M. Butterworth, F.F. Deppisch, W. Liu, A. Varma and D. Yallup

*Department of Physics and Astronomy, UCL,
Gower Street, London WC1E 6BT, U.K.*

E-mail: shyam.amrith.14@ucl.ac.uk, j.butterworth@ucl.ac.uk,
f.deppisch@ucl.ac.uk, wei.liu.16@ucl.ac.uk,
abhinav.varma.17@ucl.ac.uk, david.yallup.15@ucl.ac.uk

ABSTRACT: The large and growing library of measurements from the Large Hadron Collider has significant power to constrain extensions of the Standard Model. We consider such constraints on a well-motivated model involving a gauged and spontaneously-broken $B - L$ symmetry, within the CONTUR framework. The model contains an extra Higgs boson, a gauge boson, and right-handed neutrinos with Majorana masses. This new particle content implies a varied phenomenology highly dependent on the parameters of the model, very well-suited to a general study of this kind. We find that existing LHC measurements significantly constrain the model in interesting regions of parameter space. Other regions remain open, some of which are within reach of future LHC data.

KEYWORDS: Beyond Standard Model, Hadron-Hadron scattering (experiments), Global features, Hard scattering, Particle and resonance production

ARXIV EPRINT: [1811.11452](https://arxiv.org/abs/1811.11452)

Contents

1	Introduction	1
2	$B - L$ gauge model	2
3	Theoretical constraints and benchmark scenarios	5
3.1	Vacuum stability and perturbativity	5
3.2	Renormalisation group evolution	5
3.3	W boson mass constraint	6
3.4	Benchmark scenarios	6
4	Existing experimental constraints	8
5	LHC constraints using CONTUR	9
5.1	Exotic production and decay modes	9
5.2	Constraints in $M_{Z'}$ and g'_1	10
5.3	Constraints in M_{h_2} and $\sin \alpha$	13
6	Conclusions	16
A	Renormalization Group Equations	18

1 Introduction

The search for physics beyond the Standard Model (BSM) is one of the key motivations for the ongoing efforts at the Large Hadron Collider (LHC). Typically, signatures in a given BSM scenario, either a fully constructed ultraviolet (UV) complete model or a simplified model, are being searched through specific selection criteria optimized for a given scenario and possibly its parameters. While this approach will certainly result in the highest sensitivity, its specificity limits its application outside the initial scope. Given the large number of signatures and scenarios, it makes exploring the extensive BSM landscape a daunting task.

In this paper we instead employ a different approach that utilizes precision measurements of Standard Model (SM) signatures. The approach, called ‘Constraints On New Theories Using Rivet’ (CONTUR), uses particle-level differential measurements in fiducial regions of phase-space that are largely model-independent. This allows them to be compared to theoretically predicted BSM signatures. This approach, complementary to that of direct searches, can efficiently rule out BSM scenarios by comparing a large number of signatures with their measurements. The CONTUR method was introduced in [1] where it was applied to a simplified model of Dark Matter, and has also been applied to exotic light

scalars and to a two-Higgs-doublet model [2]. We here extend the method and apply it to a UV complete model, especially exploiting its power to test multiple signatures.

There is significant interest in extensions to the SM in which the global symmetry behind the conservation of $B - L$ (Baryon number minus lepton number) is gauged, giving an additional $U(1)_{B-L}$ symmetry and an associated new gauge boson. In the specific model in which we are interested here, this additional $U(1)_{B-L}$ gauge symmetry is spontaneously broken by an extra SM singlet Higgs. To make the model anomaly-free it also incorporates three generations of neutral leptons sterile under the SM gauge interactions, thereby enabling the Seesaw mechanism of light neutrino mass generation. A variant of the model was discussed in [3], with a focus on signatures involving displaced vertices from relatively long-lived RH neutrinos. The parameter space of $U(1)_{B-L}$ has also been studied in previous work [4–13] with focuses on different sectors of the model. In this paper we consider the potential signatures from a wider range of model parameters and processes, in which long-lived particle decays play no significant role. We use the Herwig event generator [14] to generate inclusively all signatures involving the new particle content of the model, and confront these expectations with LHC data using the CONTUR package [1] and the Rivet library [15]. This allows us to delineate regions in which LHC data already disfavour the model, and regions in which future measurements may provide sensitivity.

This paper is organized as follows. In section 2, we briefly review the $U(1)_{B-L}$ gauge model and its immediate phenomenological consequences. Section 3 then summarizes indirect theoretical considerations that constrain the relevant model parameters. In addition we here also introduce the benchmark parameter cases we study in our analysis. The important direct experimental constraints on the model are presented in section 4. Our analysis using the CONTUR approach is contained in section 5, focussing in turn on constraints on the exotic gauge and Higgs sector. We conclude with a summary of our findings and an outlook in section 6.

2 $B - L$ gauge model

In addition to the particle content of the SM, the $U(1)_{B-L}$ model contains an Abelian gauge field B'_μ , a SM singlet scalar field χ and three RH neutrinos N_i . The gauge group is $SU(3)_c \times SU(2)_L \times U(1)_Y \times U(1)_{B-L}$, where the scalar and RH neutrinos have $B - L$ charges $Y_{B-L} = +2$ and -1 , respectively. Among the SM fields, all quarks and leptons have charges $Y_{B-L} = +1/3$ and -1 , respectively, whereas all other SM fields are uncharged under $U(1)_{B-L}$. The scalar sector of the Lagrangian reads

$$\mathcal{L} \supset (D^\mu H)^\dagger (D_\mu H) + (D^\mu \chi)^\dagger D_\mu \chi - \mathcal{V}(H, \chi), \tag{2.1}$$

with the SM Higgs doublet H and the scalar potential $V(H, \chi)$ given by

$$\mathcal{V}(H, \chi) = m^2 H^\dagger H + \mu^2 |\chi|^2 + \lambda_1 (H^\dagger H)^2 + \lambda_2 |\chi|^4 + \lambda_3 H^\dagger H |\chi|^2. \tag{2.2}$$

Here, D_μ is the covariant derivative [16]

$$D_\mu = \partial_\mu + ig_s \mathcal{T}_\alpha G_\mu^\alpha + ig T_a W_\mu^a + ig_1 Y B_\mu + i(\tilde{g} Y + g'_1 Y_{B-L}) B'_\mu, \tag{2.3}$$

where G_μ^α , W_μ^a , B_μ are the usual SM gauge fields along with their couplings g_s , g , g_1 and generators \mathcal{T}_α , T_a , Y . The Abelian gauge field B'_μ couples via the $U(1)_{B-L}$ symmetry with gauge strength g'_1 to all particles carrying a $B-L$ charge Y_{B-L} . In our analysis, we omit the Abelian mixing between $U(1)_{B-L}$ and $U(1)_Y$, $\tilde{g} = 0$, as a simplification. This means we consider the minimal gauged $B-L$ model. Consequently, the SM gauge sector is extended to include the kinetic term

$$\mathcal{L} \supset -\frac{1}{4} F'^{\mu\nu} F'_{\mu\nu}, \tag{2.4}$$

with the field strength tensor of the $B-L$ field, $F'_{\mu\nu} = \partial_\mu B'_\nu - \partial_\nu B'_\mu$. This is manifest observationally as a new gauge boson, Z' , coupling to SM fermions with a characteristic coupling g'_1 .

The fermion part of the Lagrangian now contains a term for the right-handed neutrinos

$$\mathcal{L} \supset i\bar{\nu}_{Ri}\gamma_\mu D^\mu \nu_{Ri}, \tag{2.5}$$

but is otherwise identical to the SM apart from the covariant derivatives incorporating the $B-L$ gauge field. Here, a summation over the fermion generations $i = 1, 2, 3$ is implied. Finally, the Lagrangian contains the additional Yukawa terms

$$\mathcal{L} \supset -y_{ij}^\nu \bar{L}_i \nu_{Rj} \tilde{H} - y_{ij}^M \bar{\nu}_{Ri}^c \nu_{Rj} \chi + \text{h.c.}, \tag{2.6}$$

where L is the SM lepton doublet, $\tilde{H} = i\sigma^2 H^*$ and a summation over the generation indices $i, j = 1, 2, 3$ is implied. The Yukawa matrices y^ν and y^M are at this point general 3×3 matrices; RH neutrino masses M_{Ni} are generated by the breaking of the $B-L$ symmetry through the vacuum expectation value $x = \langle \chi \rangle$ as outlined below, with the mass matrix given by $M_R = \sqrt{2} y^M x$. The light neutrinos mix with the RH neutrinos via the Dirac mass matrix $m_D = y^\nu v / \sqrt{2}$, generated after EW symmetry breaking, $v = \langle H^0 \rangle$. The complete mass matrix in the (ν_L, ν_R^c) basis is then

$$\mathcal{M} = \begin{pmatrix} 0 & m_D \\ m_D & M_R \end{pmatrix}, \tag{2.7}$$

In the well studied seesaw limit, $M_R \gg m_D$, the light and heavy neutrino masses are $m_\nu \sim -m_D M_R^{-1} m_D^T$ and $M_N \sim M_R$. The flavour and mass eigenstates of the light and heavy neutrinos are connected as

$$\begin{pmatrix} \nu_L \\ \nu_R \end{pmatrix} = \begin{pmatrix} V_{LL} & V_{LR} \\ V_{RL} & V_{RR} \end{pmatrix} \begin{pmatrix} \nu \\ N \end{pmatrix}, \tag{2.8}$$

schematically written in terms of 3-dimensional blocks in generation space. The SM charged current lepton mixing $V_{LL} = U_{\text{PMNS}}$ is determined by oscillation experiments (in the basis of diagonal charged lepton masses and apart from small non-unitarity corrections) whereas the active-sterile mixing $V_{LR} \lesssim 0.1 - 0.01$ is constrained by electroweak precision data, largely independent of the RH neutrino mass. More stringent but highly mass-dependent constraints can be set from direct searches at the LHC, lepton colliders and high intensity

experiments, see [17] and references therein. For the simplifying case a single generation of light and heavy neutrinos we will consider, eq. (2.8) reduces to the 2×2 form

$$\begin{pmatrix} \nu_L \\ \nu_R \end{pmatrix} = \begin{pmatrix} \cos \theta_\nu & -\sin \theta_\nu \\ \sin \theta_\nu & \cos \theta_\nu \end{pmatrix} \begin{pmatrix} \nu \\ N \end{pmatrix}. \quad (2.9)$$

For simplicity, we thus neglect mixing among flavours and therefore generations decouple. This corresponds to a diagonal Yukawa coupling matrix $y'_{ii} = \sqrt{2}M_{N_i}V_{iN}/v$ with $i = e, \mu, \tau$ and using the neutrino seesaw relation. Here, V_{iN} represents the active-sterile mixing, $\sin \theta_i = V_{iN}$, in the three generations.

Crucial for the above to work, the $U(1)_{B-L}$ symmetry is broken by the vacuum expectation value of the additional scalar singlet χ which then also causes it to mix with the SM Higgs. The mass matrix of the Higgs fields (H, χ) at tree level is [18]

$$M_h^2 = \begin{pmatrix} 2\lambda_1 v^2 & \lambda_3 x v \\ \lambda_3 x v & 2\lambda_2 x^2 \end{pmatrix}. \quad (2.10)$$

The physical masses of the two Higgs states h_1, h_2 are then

$$M_{h_{1(2)}}^2 = \lambda_1 v^2 + \lambda_2 x^2 - (+)\sqrt{(\lambda_1 v^2 - \lambda_2 x^2)^2 + (\lambda_3 x v)^2}, \quad (2.11)$$

and the (h_1, h_2) states are related to the gauge states (H, χ) via

$$\begin{pmatrix} h_1 \\ h_2 \end{pmatrix} = \begin{pmatrix} \cos \alpha & -\sin \alpha \\ \sin \alpha & \cos \alpha \end{pmatrix} \begin{pmatrix} H \\ \chi \end{pmatrix}. \quad (2.12)$$

The directly measurable parameters for the Higgs sector are the masses M_{h_1} and M_{h_2} , as well as the mixing angle α expressed as

$$\tan(2\alpha) = \frac{\lambda_3 v x}{\lambda_2 x^2 - \lambda_1 v^2}. \quad (2.13)$$

The other measurable independent parameters can be taken to be the mass and coupling of the Z' , $M_{Z'}$, g'_1 , and the RH neutrino masses M_{N_i} .

The $U(1)_{B-L}$ model is phenomenologically appealing. With the inclusion of three copies of right-handed neutrinos it is an anomaly-free gauge theory that incorporates three different simplified scenarios through mixing with the SM singlets of the model: the Z' via its mixing with the SM Z , the extra Higgs h_2 mixing with the SM Higgs and the right-handed neutrinos N_1 mixing with the active neutrinos. Formally, any two of the above can be switched off by taking an appropriate limit to yield a simplified model with only an extra Z' , a singlet scalar or a singlet neutrino. These scenarios have been studied extensively in the literature. For example, an easy way to achieve a simplified model with only singlet neutrinos is to assume a very high $U(1)_{B-L}$ breaking scale (with vanishing Higgs and gauge mixing), but make the heavy neutrino Yukawa couplings y^M small to keep the states accessible.

3 Theoretical constraints and benchmark scenarios

While we focus on direct experimental constraints from LHC searches in this work, we still need to incorporate theoretical considerations and indirect experimental constraints to disregard parameter space that is either unphysical or where a perturbative treatment is not possible. Theoretical considerations may also hint at interesting parameter space. Below, we discuss the requirement of vacuum stability and perturbativity, both at the EW scale as well as higher scales. As the model incorporates new exotic particles, it can also affect electroweak precision observables. The most sensitive quantity in this regard is the SM W boson mass, which we consider below. We here omit constraints from perturbative unitarity which will set upper limits on the extra Higgs mass but which are generally less severe than the constraints considered above [16].

3.1 Vacuum stability and perturbativity

A basic requirement is that the vacuum is stable; this puts a constraint on the parameters in the scalar potential. As we would like to impose these constraints on observable quantities, we express the couplings for the quartic terms of the Higgs potential in eq. (2.12) as

$$\begin{aligned}\lambda_1 &= \frac{1}{4v^2}[(M_{h_1}^2 + M_{h_2}^2) - \cos 2\alpha(M_{h_2}^2 - M_{h_1}^2)], \\ \lambda_2 &= \frac{1}{4x^2}[(M_{h_1}^2 + M_{h_2}^2) + \cos 2\alpha(M_{h_2}^2 - M_{h_1}^2)], \\ \lambda_3 &= \frac{1}{2vx}[\sin 2\alpha(M_{h_2}^2 - M_{h_1}^2)]\end{aligned}\tag{3.1}$$

The vacuum stability condition then requires that [19]

$$4\lambda_1\lambda_2 - \lambda_3^2 > 0, \quad \lambda_1 > 0, \quad \lambda_2 > 0.\tag{3.2}$$

In addition, perturbativity requires the couplings in the model to be small enough such that loop corrections remain bounded. We choose the upper limit conservatively to be $|\lambda_{1,2,3}| < 1$. Our chosen model parameters are $M_{Z'}$, g'_1 , M_{h_2} , $\sin \alpha$, M_{N_i} and V_{LN} . Among these, M_N and V_{LN} do not enter to the scalar vacuum stability and perturbative constraints and we display the allowed region for each pair of parameters when setting the other pair of parameter to be a constant or some other reasonable relation. In addition to the scalar parameters, the gauge and fermion Yukawa couplings also need to remain perturbative but this simply means we restrict the relevant parameters to be $g'_1 < 1$, $M_{N_i}/x < 1$.

3.2 Renormalisation group evolution

We input parameters as shown in the table 1 at electroweak scale, then evolve all model parameters according to their respective renormalisation group equations (RGEs). Requiring that the model remains well-defined and perturbative at higher energy scales $Q > Q_{EW}$ puts additional constraints on the parameter space. If we were to assume that the $B - L$ is the ‘ultimate’ theory, i.e. not superseded by a new model at some scale Q_{UV} , we should require vacuum stability and perturbativity all the way up to the Planck scale. This is

of course a very strong theory bias and we only use it to highlight potentially interesting parameter space. In our calculations, we use the RGEs in the $B - L$ model given in [19] which is shown in the appendix A.

3.3 W boson mass constraint

An additional indirect constraint arises from the shift of the W boson mass via radiative effects of the extra Higgs in the model. This is quantified by a parameter Δr relating Fermi constant G_F , the fine structure constant α_{EM} and the electroweak renormalised gauge boson masses m_Z, m_W [20],

$$m_W^2 \left(1 - \frac{m_W^2}{m_Z^2} \right) = \frac{\pi \alpha_{EM}}{\sqrt{2} G_F} (1 + \Delta r). \tag{3.3}$$

In the SM, $\Delta r = 0.038$ which gives $m_W = 80.360$ GeV, compared to the tree level value $m_W^{\text{tree}} = 80.94$ GeV, with a theoretical uncertainty of around 4 MeV [20]. However, the experimental data gives $m_W^{\text{exp}} = 80.385 \pm 0.015$ GeV [21], which is therefore somewhat in tension with the SM prediction.

Extra particles in BSM scenarios can contribute to the mass shift. In our scenario, the singlet Higgs does so with $\Delta r = \Delta r_{SM} + \delta(\Delta r)$ leading to a mass shift

$$\Delta m_W = -\frac{1}{2} m_W \frac{\sin^2 \theta_W}{\cos^2 \theta_W - \sin^2 \theta_W} \delta(\Delta r). \tag{3.4}$$

The extra contribution $\delta(\Delta r)$ involves Higgs loops which are dependent on the masses of the two Higgs particles and their mixing angle α . The above discrepancy between the SM prediction and the observed W boson mass could be resolved if the extra Higgs is lighter than the SM Higgs [20]. We omit this possibility and instead use the above to set a constraint on the $M_{h_2} - \sin \alpha$ parameter space by requiring that the calculated m_W is within 2σ of its experimental value as described in [18].

3.4 Benchmark scenarios

There are six extra free parameters compared to the SM which can be categorised into three pairs: $M_{Z'}$ and g'_1 describing the gauge sector and also fixing the vacuum expectation value (vev) of the $B - L$ gauge; M_{h_2} and $\sin \alpha$ describing the extra Higgs mass eigenstate and the mixing between the two Higgs fields; and similarly M_{N_i} and V_{iN} for the heavy neutrino and its mixing strength with the active neutrinos. As we will describe in the next section, we largely leave aside channels incorporating heavy neutrinos, either because the discovery signal is too small as the upper bound on the neutrino mixing is $V_{iN} \lesssim 10^{-2}$ [22], or the heavy neutrino decays in a displaced vertex which cannot be captured by the CONTUR analysis in the following discussion. Thus, we safely set the neutrino masses to be $M_{N_i} = M_{Z'}/5$ in all cases. This ensures that heavy neutrino Yukawa couplings are always smaller than g'_1 . We choose V_{iN} as determined by the Type-I seesaw generation of light neutrino masses, $V_{iN} = \sqrt{\frac{m_\nu}{M_{N_i}}}$ where $m_\nu = 0.1$ eV is the mass scale of light neutrinos.

We thus focus on the other parameters where we will scan over two-dimensional slices of the parameters while keeping the other two parameters fixed. Our parameter choices are

Scenario	$M_{Z'}$ [GeV]	g'_1	M_{h_2}	$\sin \alpha$	M_{N_i}
A	$[1, 10^4]$	$[3 \times 10^{-5}, 0.6]$	$M_{Z'}/(2g'_1)$	0	$M_{Z'}/5$
B	$[1, 10^4]$	$[3 \times 10^{-5}, 0.6]$	$M_{Z'}/(2g'_1)$	0.2	$M_{Z'}/5$
C	$[1, 10^4]$	$[3 \times 10^{-5}, 0.6]$	200 GeV	0.2	$M_{Z'}/5$
D	7000	0.2	$[0, 800]$ GeV	$[0, 0.7]$	$M_{Z'}/5$
E	35	10^{-3}	$[0, 800]$ GeV	$[0, 0.7]$	$M_{Z'}/5$

Table 1. Benchmark scenarios used in our analysis. In addition, the active-sterile neutrino mixing is fixed as $V_{iN} = \sqrt{0.1 \text{ eV}/M_{N_i}}$, independent of the generation of the heavy neutrino.

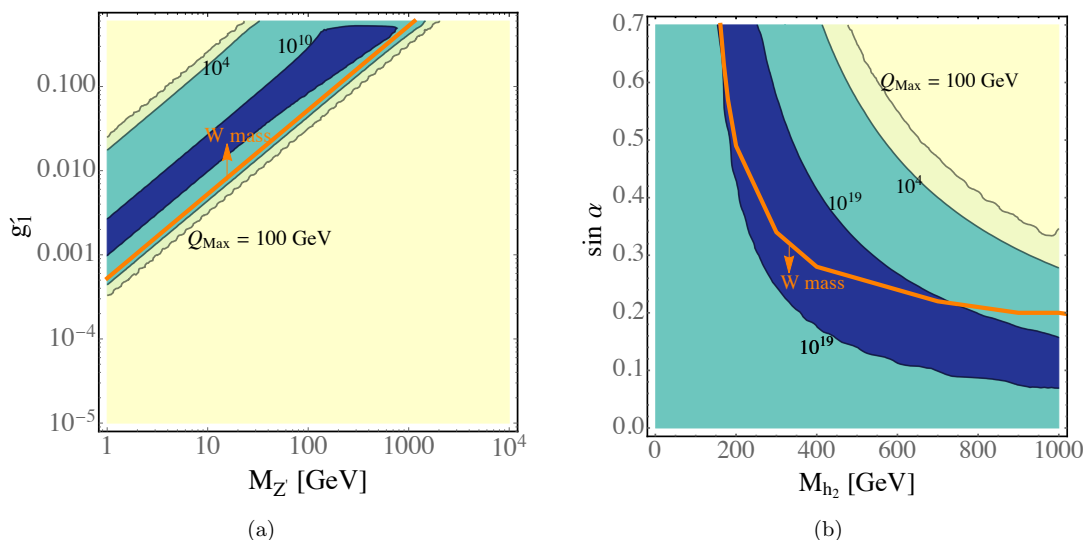


Figure 1. Maximal perturbative scale Q_{Max} in GeV and constraint from electroweak W mass corrections as a function of (a) g'_1 and $M_{Z'}$ with $M_{h_2} = M_{Z'}/(2g'_1)$ and $\sin \alpha = 0.2$ (Case B) and (b) M_{h_2} and $\sin \alpha$ with $M_{Z'} = 7 \text{ TeV}$ and $g'_1 = 0.2$ (Case D). The W mass constraint is satisfied above (below) the depicted contour in panel a (b), as indicated by the arrows.

summarised in table 1. For $M_{Z'}$ and g'_1 , we can choose to switch off the effects of the Higgs mixing and the second Higgs mass eigenstates by setting $\sin \alpha = 0$ and $M_{h_2} = M_{Z'}/(2g'_1)$ the $B - L$ gauge breaking vev x (Case A). We can also consider only the Higgs mixing by setting $\sin \alpha = 0.2$ (Case B) which is still allowed by the direct experimental limits described below and the W mass constraint [20]. Finally, we can switch on both, setting $\sin \alpha = 0.2$ and $M_{h_2} = 200 \text{ GeV}$ (Case C); while still allowed from theoretical considerations and Higgs property determinations, this choice will have stronger constraints from searches.

In choosing M_{h_2} and $\sin \alpha$, as the $B - L$ breaking scale needs to be higher than 3.45 TeV experimentally as described below, we use $g'_1 = 0.2$ and $M_{Z'} = 7 \text{ TeV}$ (Case D). Another parameter choice (Case E) can be proposed when we combine the effects of a light Z' by setting $M_{Z'} = 35 \text{ GeV}$ with $g'_1 = 10^{-3}$ yielding the same vev as Case D. This would allow a possible production channel of heavy neutrinos as many more Z' are produced, due to its light mass and subsequent decays to the lighter heavy neutrinos.

In figure 1, we show the maximal scale Q_{Max} up to which the model remains perturbative for Case B and D, as a function of the respective running model parameters. In

figure 1(a), only a narrow band from $g'_1 \approx 10^{-3}$, $M_{Z'} \approx 1 \text{ GeV}$ to $g'_1 \lesssim 1$, $M_{Z'} \approx 1 \text{ TeV}$ permits Q_{Max} as high as 10^{10} GeV . This is an indirect effect as the extra Higgs mass is adjusted as $M_{h_2} = \frac{M_{Z'}}{2g'_1}$ while $\sin \alpha = 0.2$ is kept at a constant and fairly high value. This behaviour becomes clearer for Case D, depicted in figure 1(b). Here, perturbativity rules out simultaneously large M_{h_2} and $\sin \alpha$ but it permits a hyperbolic band where Q_{Max} is at or above the Planck scale. In addition, the constraint from the W boson mass corrections is shown in both plots as well. In figure 1(a), the allowed region from this consideration is *above* the depicted line while in figure 1(b), the region *below* the corresponding line is allowed.

4 Existing experimental constraints

Before analyzing the constraints from LHC SM searches using the CONTUR framework, we here briefly summarize other experimental constraints on the model parameters - in particular, the additional gauge boson mass $M_{Z'}$, the $B - L$ gauge coupling g'_1 , the Higgs mixing angle $\sin \alpha$, the second Higgs mass M_{h_2} and the RH neutrino mass M_{N_i} .

For $M_{Z'}$ and g'_1 , the experimentally sensitive parameter is the vev of the $B - L$ gauge-breaking Higgs. Resonance searches in $pp \rightarrow Z' \rightarrow l^+l^-$ bound the Z' mass to $M_{Z'} \gtrsim 4.5 \text{ TeV}$ [23, 24] with a SM-valued gauge coupling. Searches at LEP-II [25–28] for a resonance constrain Z' mass and gauge coupling, and thus the $B - L$ breaking scale $x \equiv M_{Z'}/(2g'_1) \geq 3.45 \text{ TeV}$. Thus for Cases D and E, the vev 17.5 TeV we have selected is allowed. For Case A, this limit lies within the region subsequently excluded by LHC dilepton searches.

A constraint applicable to the whole range of Z' masses we consider here is provided through the measurement of the electron-neutrino cross section principally from Charm II [13, 29], obtained via the *Darkcast* framework [12].

Searches for dark photons can be recast to other BSM models, and the *Darkcast* framework can use these to provide the corresponding limits for the $B - L$ model [12]. This extends the current experimental limits on g'_1 for low $M_{Z'}$, such that $g'_1 < 10^{-4}$ for $M_{Z'} \leq 10 \text{ GeV}$ and $g'_1 \lesssim 10^{-3}$ for $10 \text{ GeV} < M_{Z'} < 70 \text{ GeV}$. The latter region is dominated by the LHCb dark photon search [30]. As the Higgs mixing $\sin \alpha$ is not considered in the production mechanisms, these limits cannot be directly applied to Case B or C, although they can be expected to have some impact.

The SM singlet Higgs and its mixing angle α with the SM Higgs are constrained by perturbativity and unitarity considerations [16], setting an upper limit on M_{h_2} as described above. Additionally, direct searches at the LHC for a BSM Higgs signal further constrain the mixing such that $\sin \alpha \lesssim 0.35$ in the aforementioned mass range [31]. An indirect constraint on the Higgs mixing angle $\sin^2 \alpha \lesssim 0.31$ can also be obtained from the measurement of SM Higgs decays into a number of SM final states [32, 33]. The bound coming from SM Higgs signal strength measurement is valid for all masses of the BSM Higgs $M_{h_2} > M_{h_1}$.

In the present work, we consider relatively low mass right-handed neutrinos, $M_N = M_{Z'}/5$, in order to ensure there are decay channels open to the h_2 in all scenarios. This means that RH neutrinos may be pair-produced from Z' decays. In a pure Type-I seesaw

scenario, the RH neutrino mass is related to the mixing with the active neutrinos and the light neutrino mass via $M_{Ni} \sim \frac{m_\nu}{V_{iN}^2}$. The sub-eV scale light neutrino mass constraints from $0\nu\beta\beta$ and Tritium beta decay experiments as well as from cosmological observations such as Planck [34, 35] together with the maximal active-sterile mixing $V_{iN} \sim 0.01$ limited by direct searches (see e.g. [17] and references therein) gives a lower limit $M_{Ni} > 1$ keV which is easily satisfied in the $M_{Z'}$ region we choose.

5 LHC constraints using CONTUR

Our analysis proceeds as follows. The Lagrangian for the model is coded in Feynrules [36] and used to produce a UFO [37] file, which is then read into Herwig7 [14].¹ All tree-level processes involving one or more BSM particles (N, Z', h_2) in the matrix element are generated in proton-proton collisions at 7, 8 and 13 TeV. The effective Higgs couplings to gluons and photons via loops are also included. Any interference terms between BSM and SM contributions to final states are neglected. Unstable particles are decayed by Herwig. QCD and QED radiation are simulated using a leading-logarithmic shower. Underlying event, hadronisation and hadron decays are also simulated, to produce a realistic event final state. These events are passed to Rivet [15], so that their contribution to the fiducial regions of LHC measurements, from ATLAS, CMS and LHCb, can be evaluated. This is possible because the measurements are defined in terms of idealised final-state particles and corrected for detector effects. This is done within fiducial regions in which the detector has high acceptance, a procedure which minimises model dependence. The significance of the additional BSM contributions relative to the experimental uncertainties on the measurements is used to derive a confidence level (CL) at which the given BSM parameter point is disfavoured, on the assumption that the measurement is equal to the SM. This comparison is made using CONTUR [1] and is roughly equivalent to treating all the measurements (which have been shown to agree with the SM) as data-driven control regions. A simple χ^2 test statistic is used, the confidence interval is calculated for the different signal hypotheses using asymptotic distributions of the test statistic [38] and interpreted as a CL using the CL_s formalism [39]. Statistical correlations are eliminated by only taking the most significant point from any data set where there are overlaps of events. Systematics are assumed to be 100% correlated within a distribution and uncorrelated between distributions.

5.1 Exotic production and decay modes

The relevant production and decay modes vary depending upon the parameters of the model. However, the most important are

- the direct production of Z' , (or for lower masses, multiple Z'), often in association with hadronic jets, and with subsequent Z' decay to leptons
- the decay of the SM Higgs to Z' pairs.

¹Version 7.1.4, changeset 0d744493e50e is used for the limit plots. Version 7.1.2 is used for the RH neutrino lifetime only.

- production of the h_2 via gluon fusion, with subsequent decay to weak bosons.
- production of the h_2 via gluon fusion, with subsequent decay to Z' .
- associated production of the h_2 or Z' with γ , W or Z .

The RH neutrino masses are all set to $M_{N_i} = M_{Z'}/5$, and these neutrinos may also be produced. Their proper decay length $c\tau \approx 2.5 \times 10^5 \text{ m} \times (\frac{1 \text{ GeV}}{M_{N_i}})^4$, for $1 \text{ GeV} \ll M_{N_i} < M_W$, will vary across the parameter space, as shown as an example for Case B in figure 2(a). For low $M_{Z'}$ (and hence low M_{N_i}), $c\tau > 10\text{m}$ and the neutrinos may be considered to be stable for our purposes. However as $M_{Z'}$ increases above the Z mass, $c\tau$ decreases, leading first to displaced decays within the detector volume, and eventually to effectively prompt decays. The CONTUR approach is not well-suited to considering displaced vertex decays, since the fiducial cross section definitions and the detector corrections applied to obtain them typically consider only prompt particles (or in specialised cases, weak decays of SM particles such as B-hadrons or τ leptons). Thus in the present analysis, the RH neutrinos are artificially set to be stable, and will manifest themselves as missing transverse energy. They will therefore show as missing energy contributions in the fiducial cross sections. For low M_{N_i} , this is a good approximation, as seen in figure 2(a). For higher neutrino masses, the neutrino should decay, but for most of the parameter space the production cross section is very low, as can be seen in figure 2(b). The exception is at high g'_1 , but in this region the contribution from other signatures is also large, and over all the parameter region the contribution to the CONTUR sensitivity from signatures involving heavy neutrinos is negligible. Taking advantage of displaced vertex signatures is likely to require dedicated searches, and may give additional sensitivity where the more conventional signatures fail, as discussed in [3].

5.2 Constraints in $M_{Z'}$ and g'_1

For Case A, the BSM Higgs sector is effectively decoupled by setting $\alpha = 0$, and M_{h_2} is set equal to $\frac{M_{Z'}}{2g'_1}$ which also ensures vacuum stability (see section 3.1). We study the parameter space in $M_{Z'}$ and g'_1 , with $M_{Z'}$ and g'_1 scanned over the ranges $1 \text{ GeV} < M_{Z'} < 10 \text{ TeV}$ and $3 \times 10^{-5} < g'_1 < 0.6$.

These settings make our model phenomenologically very similar to the scenario discussed by Batell, Pospelov and Shuve [40], and our limits, shown in figure 3(a) can be compared to their figure 3, as well as to the more recent figure 5 of [12]. In this scenario, the whole plane is allowed by the theoretical constraints of section 3.1, and the W mass constraint has no impact. The LHC data considered in CONTUR disfavour most of the region for $g'_1 > 0.01$ for $M_{Z'} < 2 \text{ TeV}$, and have little sensitivity below this. The exclusion comes dominantly from the leptonic decays of the Z' , which would have appeared in various leptonic differential cross sections, and are absent in the data. The ATLAS 7 and 8 TeV Drell-Yan measurements [41–43] have a big impact for $12 \text{ GeV} < M_{Z'} < 1500 \text{ GeV}$, with the WWW cross section [44] also having an impact at the highest $M_{Z'}$. As expected, our sensitivity tracks that of the ATLAS 13 TeV search, also shown, which naturally does even better at high $M_{Z'}$, given the higher beam energy. No particle-level measurement for

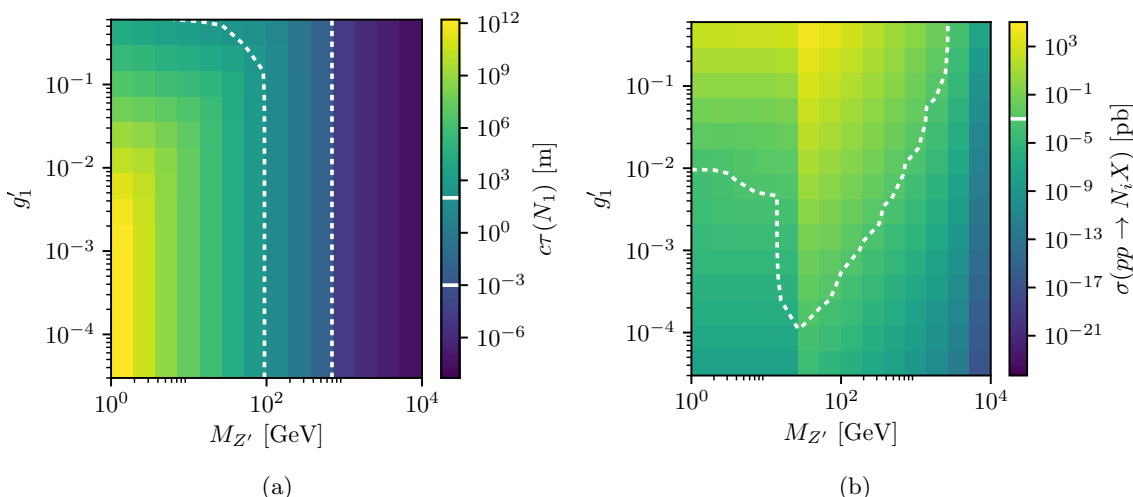


Figure 2. (a) The proper decay length of the heavy RH neutrino for Case B. The dashed lines indicate the boundaries of region between $100 \text{ m} > c\tau > 1 \text{ mm}$ within which the neutrino would manifest a “long-lived particle” signal. (b) the total production cross section for the RH neutrino in Case B, for 8 TeV pp collisions. The dashed line indicates the 1 fb contour, corresponding to roughly 30 events before any cuts, for the maximum luminosity considered here.

this final state in 13 TeV collisions is available in Rivet at time of writing. The Z +jets measurements [45, 46] also disfavour the model in some of this region. As can be seen, the sensitive region was largely already excluded by the combination of electron-neutrino cross section measurements and LHC search data. However, there are regions around $70 < M_{Z'} < 150 \text{ GeV}$, where the limits from current data are weaker (except for a very narrow exclusion around the Z mass from LEP, not shown). LHC measurements are able to fill in this window.

Next we consider Case B, in which the h_2 mixes with the SM Higgs via a mixing angle of $\sin \alpha = 0.2$. The sensitivity plot is shown in figure 3(b). The electron-neutrino scattering limit still applies, although introduction of an h_2 mixing can in principle alter the production and decay of the Z' , so the ATLAS dilepton limit does not obviously apply without modification. It can be seen, however, that the CONTUR limit derived from the 8 TeV dilepton measurement does not change at high $M_{Z'}$ and high g_1' , so it is reasonable to assume the ATLAS limit of figure 3(a) would also be unchanged.

More significantly, in Case B, the theory constraints come into play, and everything outside the purple coloured lines (i.e. the majority of the parameter plane) is ruled out by requiring that the models remain perturbative at least to a scale of 10 TeV, details on the derivation of this are discussed in section 3.4 and shown explicitly for Case B in figure 1(a). This scale choice is displayed as it is deemed to define at least a safe region for the energy scales probed at the LHC. The electron-neutrino scattering limit still applies, and the W Mass constraint also excludes most of the plane for high $M_{Z'}$ and lower g_1' . Only a narrow region remains, along a band from $M_{Z'} \approx 200 \text{ GeV}$ at $g_1' = 0.6$ to $g_1' \approx 0.002$ at $M_{Z'} = 1 \text{ GeV}$. The CONTUR analysis of LHC data disfavors this entire band.

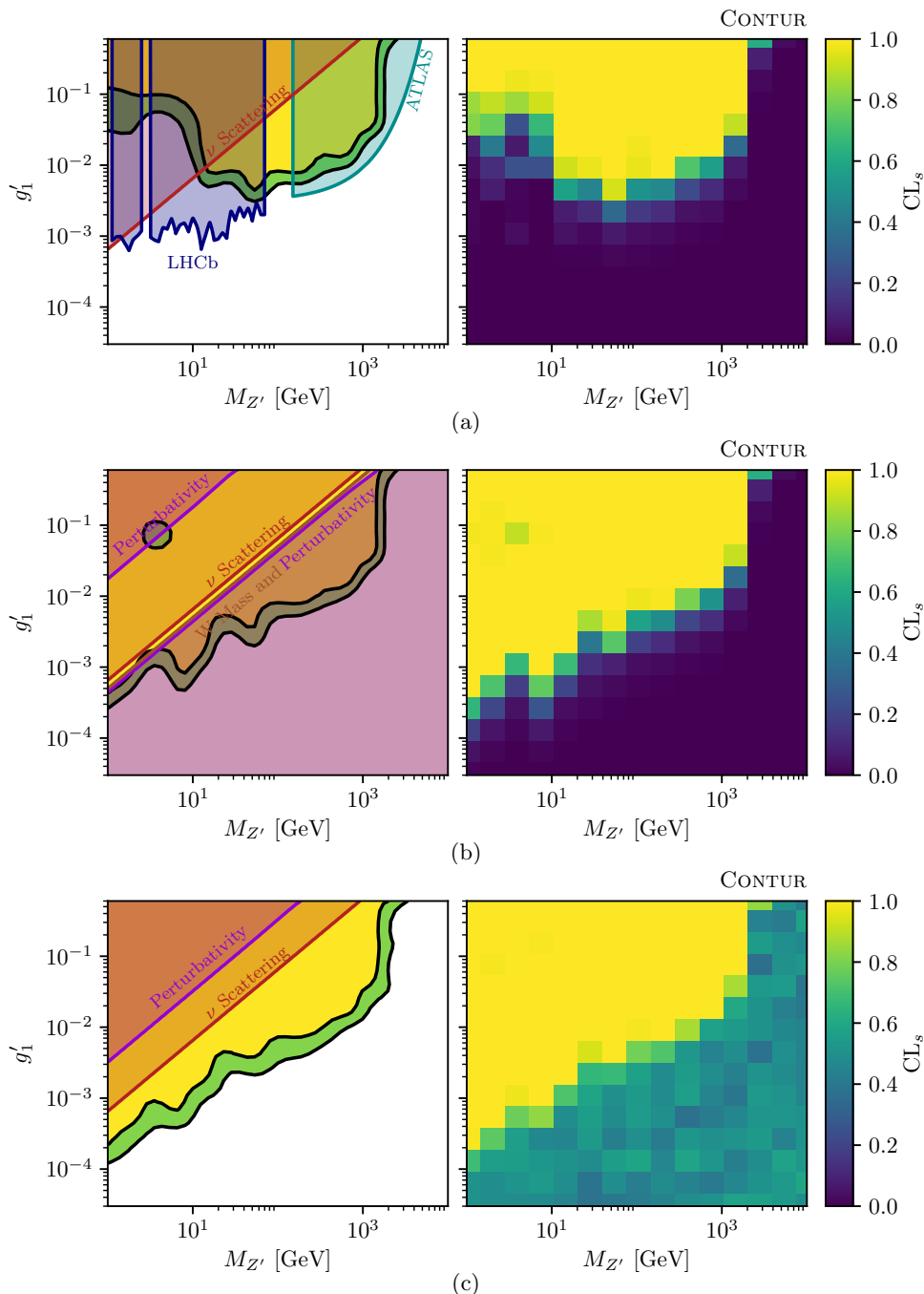


Figure 3. Sensitivity of LHC measurements to the BSM contribution from a gauged B-L model in the $M_{Z'}$ vs g_1' plane. (a) Case A, $\sin \alpha = 0$, $M_{h_2} = \frac{M_{Z'}}{2g_1'}$; left, 95% (yellow) and 68% (green) excluded contours. Right, underlying heatmap of exclusion at each scanned parameter space point. The 95% CL limits from the ATLAS search using lepton pairs [23], from electron-neutrino scattering, from the Darkcast reinterpretation [12] of the LHCb dark photon search [30] and the vacuum stability and perturbativity constraints up to a scale of at least 10 TeV are also indicated; (b) Case B, $\sin \alpha = 0.2$, $M_{h_2} = \frac{M_{Z'}}{2g_1'}$; as in (a) but for Case B, with additional theory bounds and constraints from M_W and electron-neutrino scattering shown; (c) Case C, $\sin \alpha = 0.2$, $M_{h_2} = 200$ GeV; as in (b) but for Case C.

Cases with fixed M_{h_2} were also considered. If M_{h_2} is set to 1 TeV, the whole plane is excluded if perturbative constraints are applied. The experimental sensitivity is very similar to the case where $M_{h_2} = \frac{M_{Z'}}{2g_1}$. For Case C, with $M_{h_2} = 200$ GeV, the theoretically allowed region in g_1' and $M_{Z'}$ expands again, such that the only theoretically disfavoured region is that already disfavoured by electron-neutrino scattering measurements. The LHC data disfavour a similar region to Case B, as shown in figure 3(c). Notable in the heatmap of figure 3(c) is the fact there is some sensitivity, albeit weak, over the whole plane. This is primarily due to the cross section for h_2 production (via gluon fusion) followed by h_2 decay to WW , and is thus largely insensitive to $M_{Z'}$ and g_1' . These events make a significant contribution in the phase space of the $l\nu$ -jet-jet measurement of [44]. Other signatures involving leptonic decays of W and/or Z also contribute in various regions. The ATLAS 7 TeV four-lepton measurement [49] is particularly important for disfavoured the region where $M_{Z'}$ is small and g_1' is above 10^{-3} , since in this region the dominant decay of the h_2 is to Z' pairs and the branching fractions $Z' \rightarrow \mu^+\mu^-$ and $Z' \rightarrow e^+e^-$ are both around 20%. Although the Z' is well below the mass window of the Z or even Z^* in the measurement, combinatorials still populate the fiducial region. Given all of this, one can expect this region to be addressed by future LHC measurements, with increased luminosity and beam energy.

As an illustration of how multiple measurements come into play in different regions, in figure 4 the exclusion bounds for some of the different, statistically independent, classes of data used by CONTUR are shown. It may be seen that the measurements sensitive to the Z' still play a role, but the sensitivity is extended to lower values, and the four-lepton [47–49] measurements contribute to this (see e.g. figure 4(b)). The main change in this scenario is that for low $M_{Z'}$, the decay branching ratio of the both the SM Higgs and h_2 to Z' is significant, and the leptons from the Z' decay appear in the fiducial phase space of several measurements. Of course, the ATLAS and CMS measurements of Higgs properties, which are not used by CONTUR, would also rule out some of these scenarios.

Going even further into detail, figure 5 shows examples of some of the distributions which have exclusion power for this scenario. In 5a, single Z' production dominates, except for the highest mass point where combinatorials from multilepton events from Z' and h_2 production contribute. In 5b, for low $M_{Z'}$, pair production (including from h_2 decays) dominates, while for higher $M_{Z'}$, $Z' + h_2$ production contributes. In 5c, there is a powerful exclusion when $M_{Z'}$ is within the Z mass window of the analysis. Other data, including the dimuon mass, but also for example the 8 TeV $Z + \gamma$ results [50], see figure 4(d), also play a role. The cross sections and branching ratios calculated by Herwig for the most important processes are given in table 2 for each of the parameter points of figure 5.

5.3 Constraints in M_{h_2} and $\sin \alpha$

Another interesting possibility is Case D, where the Z' is heavy, and thus decouples, but the h_2 mixes significantly with the SM Higgs. In this case the mixing has a negligible effect on the SM Higgs branching ratios, and the sensitivity of the cross section measurements used by CONTUR relies upon h_2 production. Figure 6(a) shows the plane in M_{h_2} and $\sin \alpha$. The upper right portion of the plane is excluded by constraints on M_W , while perturbativity constraints, requiring the model to be perturbative and stable up to at

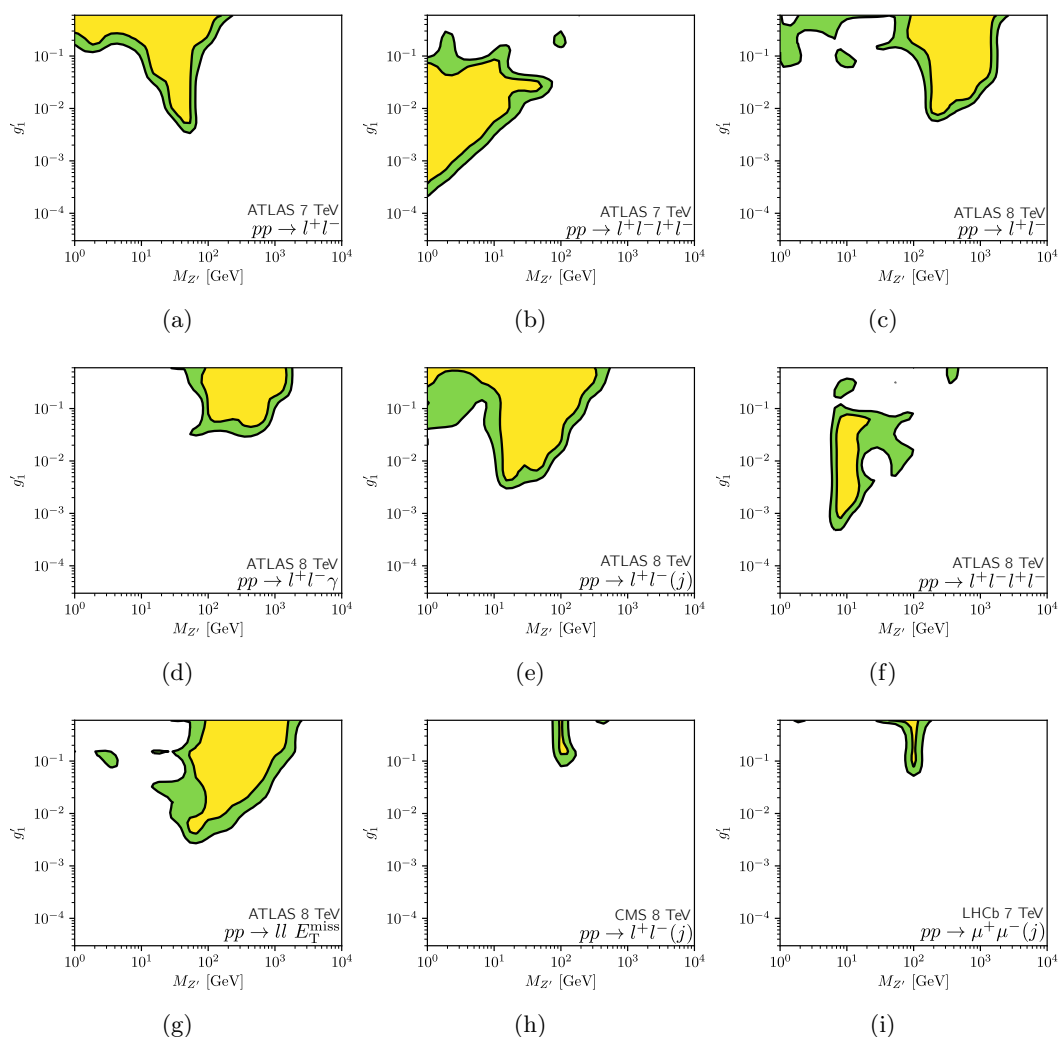


Figure 4. Disfavoured regions for different, independent measurement classes for Case C. (a) ATLAS 7 TeV Low mass Drell-Yan measurement [41], (b) ATLAS 7 TeV Four-lepton measurements [49], (c) ATLAS 8 TeV High mass Drell-Yan measurement [43], (d) ATLAS 8 TeV dilepton plus photon measurements [50], (e) ATLAS 8 TeV Dilepton plus jet measurements [42, 51, 52], (f) ATLAS 8 TeV Four-lepton measurements [48, 53], (g) ATLAS 8 TeV Dilepton plus missing transverse energy measurements [44, 54], (h) CMS 8 TeV dilepton plus jet measurements [55], (i) LHCb 7 TeV dimuon plus jet measurement [56].

least 10 TeV, eliminate a smaller region in the top right. The LHC measurements have some sensitivity at larger mixing angles ($\sin \alpha \geq 0.4$), centred on the $h_2 \rightarrow WW, ZZ$ threshold at ≈ 200 GeV, and the $h_2 \rightarrow t\bar{t}$ threshold at around 400 GeV. The most sensitive measurements here are the two-lepton-plus-two-jet cross section from [44] and the four-lepton cross section of [47]. The heat map in figure 6(a) indicates that LHC data do have some sensitivity reach at other M_{h_2} values and lower $\sin \alpha$, so that more of the parameter space is likely to become accessible if the precise measurements are made. Such measurements should be made as the LHC accumulates more integrated luminosity.

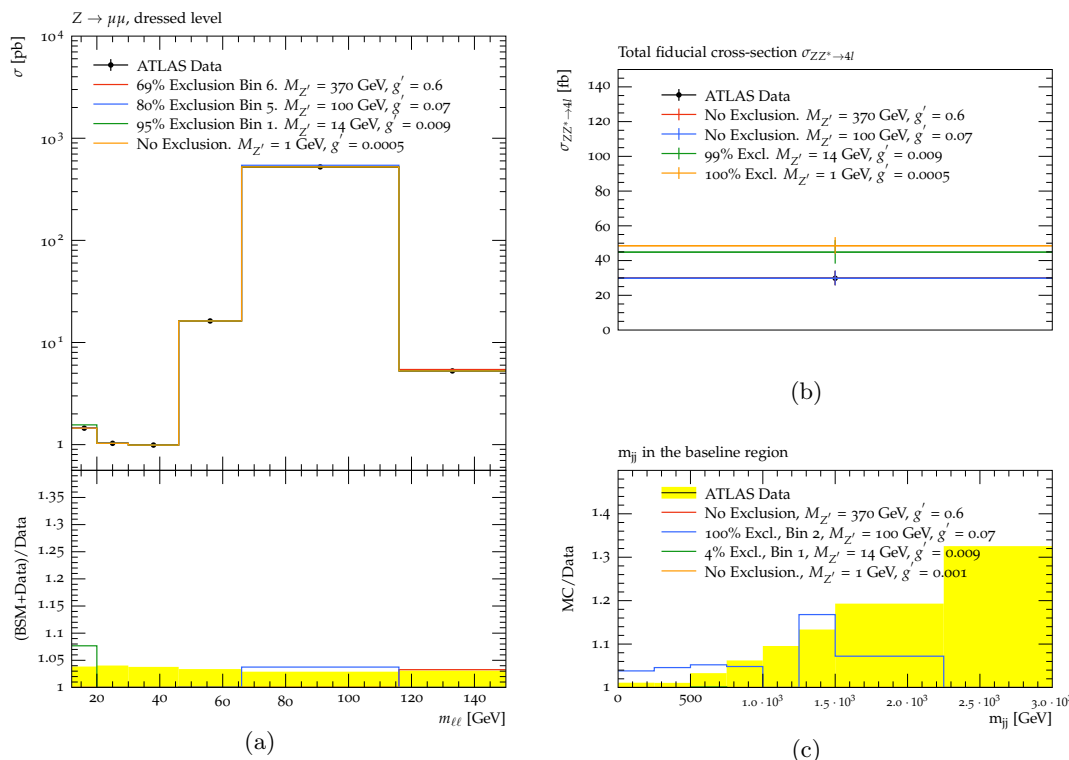


Figure 5. Examples of the exclusion from four points in the parameter space moving along the below the region of Case C excluded by neutrino scattering, figure 3(c). (a) The dimuon mass measurement from [42], (b) The ZZ^* (four lepton) measurement from [49], (c) The dijet mass in Z events from [51]. The legend indicates the parameter point in $M_{Z'}$ and g'_1 space and the bin of the plot which gives the sensitivity. $M_{h_2} = 200$ GeV

$M_{Z'}$ (GeV)	g'_1	Production Process	Cross Section (σ , pb)	Decay	Branching Fraction
1	0.0005	$gg \rightarrow Z'Z'$	0.6	$Z' \rightarrow l^+l^-$	0.36
		$gg \rightarrow gh_2$	0.078	$h_2 \rightarrow Z'Z'$	0.58
14	0.009	$u\bar{u} \rightarrow gZ'$	40.6	$Z' \rightarrow l^+l^-$	0.27
100	0.07	$u\bar{u} \rightarrow Z' \rightarrow l^+l^-$	31	$Z' \rightarrow l^+l^-$	0.27
370	0.6	$u\bar{u} \rightarrow Z' \rightarrow l^+l^-$	30	$Z' \rightarrow l^+l^-$	0.27

Table 2. Cross sections (in 8TeV pp collisions) and branching fractions for the main processes contributing to figure 5.

In some sense, Case E is complementary, and is shown in figure 6(b). $M_{Z'}$ is now low, but Z' production is now suppressed by fixing a low value of g'_1 . The exclusion derived from CONTUR is similar to Case D, but varies at lower M_{h_2} values as the decay $h_2 \rightarrow Z'Z'$ can continue to have an impact to lower M_{h_2} .

The most important processes contributing for these parameter points are summarised in table 3. Finally it should be noted that when M_{h_2} is near or below the SM Higgs mass,

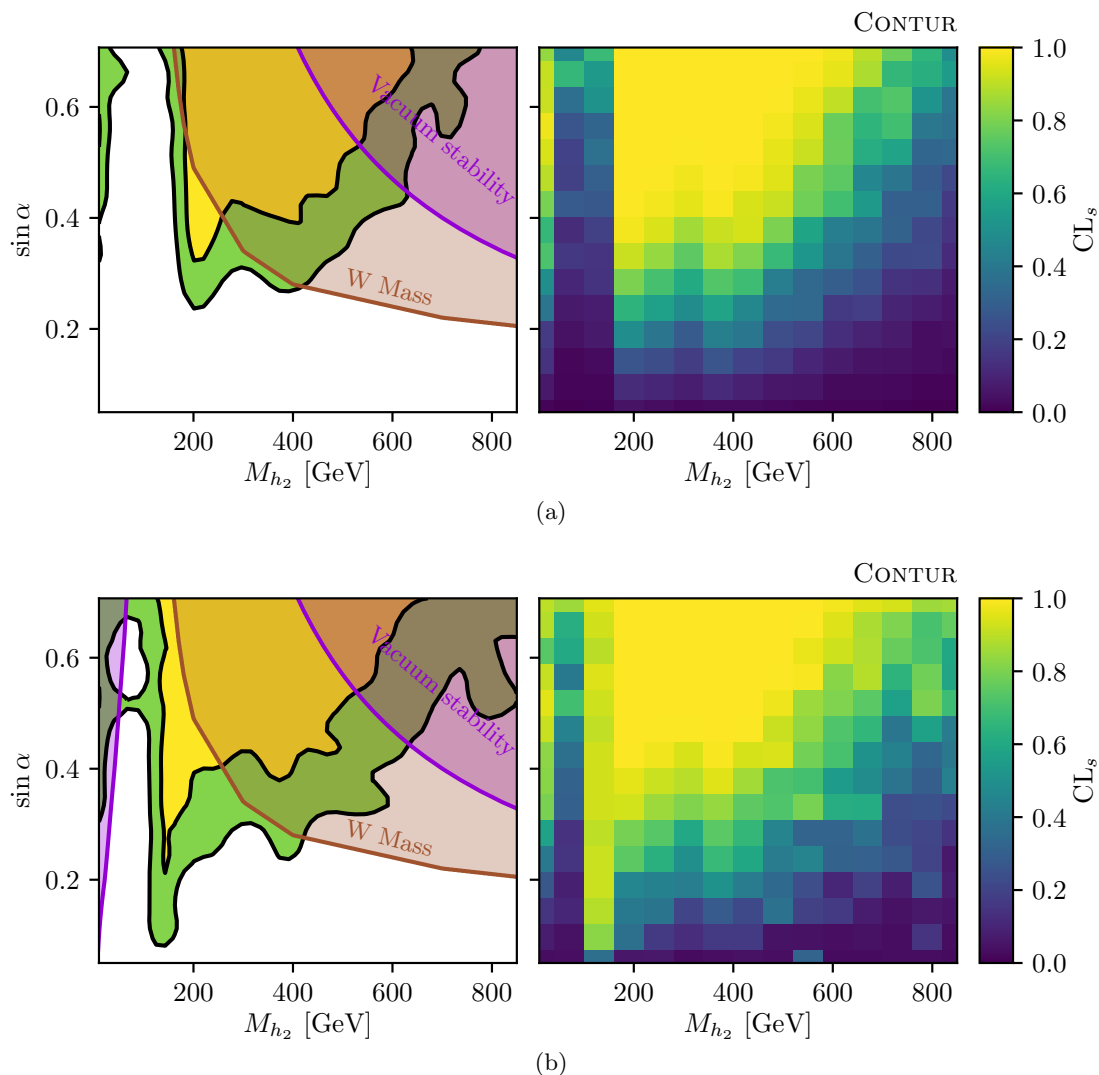


Figure 6. Sensitivity of LHC measurements to the BSM contribution from a gauged B-L model in the M_{h_2} vs $\sin \alpha$ plane, (a) Case D, $g'_1 = 0.2$, $M_{Z'} = 7$ TeV. Left, 95% (yellow) and 68% (green) excluded contours. Right, underlying heatmap of exclusion at each scanned parameter space point. The theory constraints from perturbativity and vacuum stability, requiring the model to be well behaved up to at least 10 TeV, as well as the constraint from M_W are also shown. (b) Case E, $g'_1 = 0.001$, $M_{Z'} = 35$ GeV. Figures as in (a) but for Case E.

there will be a significant impact on SM Higgs signatures which are not considered in the CONTUR analysis but which are likely to disfavour much of the parameter space for $M_{h_2} \lesssim 150$ GeV when the Higgs mixing is significant.

6 Conclusions

The new particles and interactions implied by a model based on gauging the baryon number minus lepton number $B-L$ symmetry are simulated across a wide range of parameter space for proton-proton collisions at the LHC. For significant regions of parameter space, the

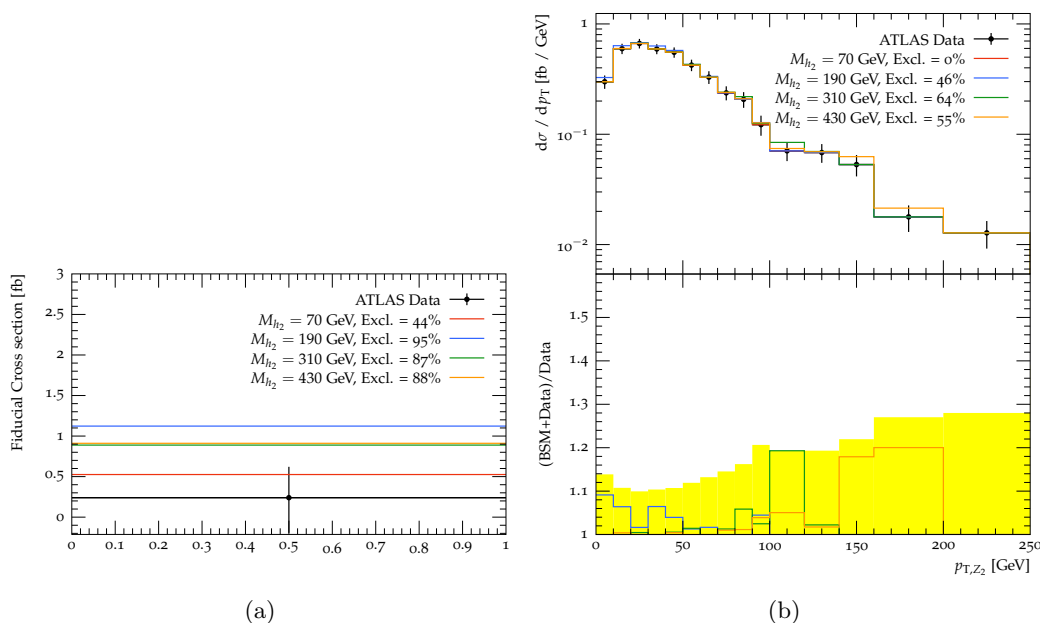


Figure 7. Examples of the exclusion from four points in the parameter space moving along the lower edge of the theoretically allowed region of figure 6(a). (a) The dilepton plus dijet measurement from [44], (b) The ZZ^* (four lepton) measurement from [47], The legend indicates the parameter point in $M_{Z'} = 7 \text{ TeV}$, $g'_1 = 0.2$, $\sin \alpha = 0.42$

M_{h_2} (GeV)	Production Process	Cross Section (σ , pb)	Decay	Branching Fraction
70	$u\bar{u} \rightarrow Zh_2$	0.13	$h_2 \rightarrow b\bar{b}$	0.88
190	$gg \rightarrow gh_2$	0.37	$h_2 \rightarrow WW$ $h_2 \rightarrow ZZ$	0.78 0.21
310	$gg \rightarrow gh_2$	0.20	$h_2 \rightarrow WW$ $h_2 \rightarrow ZZ$ $h_2 \rightarrow hh$	0.51 0.27 0.22
430	$gg \rightarrow gh_2$	0.14	$h_2 \rightarrow WW$ $h_2 \rightarrow ZZ$ $h_2 \rightarrow hh$ $h_2 \rightarrow t\bar{t}$	0.46 0.22 0.21 0.11

Table 3. Cross sections (in 8 TeV pp collisions) and branching fractions for the main processes contributing to figure 7.

new interactions contribute to signatures and phase space in which LHC measurements have already been made and in which the data have been shown to agree well with the SM. Thus in these regions the model is disfavoured or excluded already.

When the exotic Higgs of the model (h_2) is decoupled, the phenomenology is rather simple and the main sensitivity comes from the production of the new gauge boson, Z' and

its decays to leptons. In this case, our results at high $M_{Z'}$ reproduce those of resonance searches made by ATLAS and CMS in the same data set. At lower $M_{Z'}$ and for couplings g'_1 greater than about 7×10^{-3} , some previously unexamined parameter space is excluded compared to the summary of [40], in the region around $10 < M_{Z'} < 30$ GeV and around the Z mass.

If the exotic Higgs sector mixes with the SM Higgs, with a mixing angle α , we show that the sensitivity in the LHC data at high $M_{Z'}$ is retained, and that the sensitivity now extends to lower g'_1 ; for $\sin \alpha \gtrsim 0.2$ the model is disfavoured for values of g'_1 above about 5×10^{-3} for a wide range of M_{h_2} . This extension is driven by the decays of the h_2 , principally to W bosons, although for low $M_{Z'}$ the decays of the SM Higgs to Z' pairs are also important, and considering both these channels and the Z' decays to leptons in combination gives a more powerful limit than previously obtained. This is only possible because of the wide array of experimental signatures which can be considered in parallel using CONTUR.

If the Z' is suppressed either because $M_{Z'}$ is high or g'_1 is low, the sensitivity comes entirely from the extended Higgs sector. The limit on $\sin \alpha$ for this specific model using existing measurements is similar to that obtained by combining Higgs searches and Higgs signal rates in general extended scalar-sector models [34]. For $\sin \alpha < 0.2$ and $g'_1 < 5 \times 10^{-3}$, substantial regions of parameter space remain open, even for low $M_{Z'}$.

Some sensitivity, below 95% exclusion, is seen at lower $\sin \alpha$ and higher M_{h_2} values. The studies presented here use only the relatively small fraction of LHC data currently available as fiducial, particle-level measurements in HEPDATA and Rivet. As more data are collected, and increasingly precise measurements are made available in this manner, the sensitivity will grow into these further regions.

Acknowledgments

This work has received funding from the European Union’s Horizon 2020 research and innovation programme as part of the Marie Skłodowska-Curie Innovative Training Network MCnetITN3 (grant agreement no. 722104). We thank Ben Waugh for useful discussions early on in the project, and Peter Richardson for improvements and enhancements of the Herwig UFO interface.

A Renormalization Group Equations

The Renormalisation Group Equations (RGEs) for the minimal $SU(3) \times SU(2)_L \times U(1)_Y \times U(1)_{B-L}$ model are given in [19]. We here list the relevant RGEs for the convenience of the reader. The RGEs for the gauge coupling constants g_1 (associated with $U(1)_Y$), g ($SU(2)_L$), g_s ($SU(3)$) and g'_1 ($U(1)_{B-L}$) are given by

$$16\pi^2 \frac{d}{dt} g_1 = \frac{41}{6} g_1^3, \tag{A.1}$$

$$16\pi^2 \frac{d}{dt} g = -\frac{19}{6} g^3, \tag{A.2}$$

$$16\pi^2 \frac{d}{dt} g_s = -7g_s^3, \tag{A.3}$$

$$16\pi^2 \frac{d}{dt} g_1' = 12g_1'^3 + \frac{32}{3} g_1' \tilde{g} + \frac{41}{6} g_1'^2 \tilde{g}^2, \tag{A.4}$$

$$16\pi^2 \frac{d}{dt} \tilde{g} = \frac{41}{6} \tilde{g}(\tilde{g}^2 + 2g_1'^2) + \frac{32}{3} g_1'(\tilde{g}^2 + g_1'^2) + 12g_1'^2 \tilde{g}. \tag{A.5}$$

The last line describes the mixing between the U(1) terms U(1)_Y and U(1)_{B-L}.

In the Yukawa sector, we only include the effect of the large top quark Yukawa coupling Y_t and the (potentially large) Yukawa coupling y_i^M of the right-handed neutrino to the singlet scalar χ . They are given by

$$16\pi^2 \frac{d}{dt} Y_t = Y_t \left[\frac{9}{2} Y_t^2 - 8g_s^2 - \frac{9}{4} g^2 - \frac{17}{12} g_1'^2 - \frac{17}{12} \tilde{g}^2 - \frac{2}{3} g_1' - \frac{5}{3} \tilde{g} g_1' \right] \tag{A.6}$$

$$16\pi^2 \frac{d}{dt} y_i^M = y_i^M [4(y_i^M)^2 + 2Tr[(y^M)^2] - 6g_1'], \tag{A.7}$$

where, for simplicity, we assume diagonal right-handed neutrino Yukawa couplings $y_{ij}^M = y_i^M \delta_{ij}$.

Finally, the RGEs for the couplings in the scalar sector, $\lambda_1, \lambda_2, \lambda_3$, are given by

$$16\pi^2 \frac{d}{dt} \lambda_1 = 24\lambda_1^2 + \lambda_3^2 - 6Y_t^4 + \frac{9}{8} g^4 + \frac{3}{8} g_1'^4 + \frac{3}{4} g^2 g_1'^2 + \frac{3}{4} g^2 \tilde{g}^2 + \frac{3}{4} g_1'^2 \tilde{g}^2, \\ + \frac{3}{8} \tilde{g}^4 + 12\lambda_1 Y_t^2 - 9\lambda_1 g^2 - 3\lambda_1 g_1'^2 - 3\lambda_1 \tilde{g}^2, \tag{A.8}$$

$$8\pi^2 \frac{d}{dt} \lambda_2 = 10\lambda_2^2 + \lambda_3^2 - \frac{1}{2} Tr[(y^M)^4] + 48g_1'^4 + 4\lambda_2 Tr[(y^M)^2] - 24\lambda_2 g_1'^2, \tag{A.9}$$

$$8\pi^2 \frac{d}{dt} \lambda_3 = \lambda_3 \left(6\lambda_1 + 4\lambda_2 + 2\lambda_3 + 3Y_t^2 - \frac{3}{4} (3g - g_1'^2 - \tilde{g}^2) + 2Tr[(y^M)^2] - 12g_1'^2 \right) \\ + 6\tilde{g}^2 g_1'^2. \tag{A.10}$$

Open Access. This article is distributed under the terms of the Creative Commons Attribution License ([CC-BY 4.0](https://creativecommons.org/licenses/by/4.0/)), which permits any use, distribution and reproduction in any medium, provided the original author(s) and source are credited.

References

- [1] J.M. Butterworth et al. *Constraining new physics with collider measurements of Standard Model signatures*, *JHEP* **03** (2017) 078 [[arXiv:1606.05296](https://arxiv.org/abs/1606.05296)] [[INSPIRE](#)].
- [2] G. Brooijmans et al., *Les Houches 2017: physics at TeV colliders new physics working group report*, in *Les Houches 2017: physics at TeV colliders new physics working group report*, June 5–23, Les Houches, France (2018), [arXiv:1803.10379](https://arxiv.org/abs/1803.10379) [[INSPIRE](#)].
- [3] F.F. Deppisch, W. Liu and M. Mitra, *Long-lived heavy neutrinos from Higgs decays*, *JHEP* **08** (2018) 181 [[arXiv:1804.04075](https://arxiv.org/abs/1804.04075)] [[INSPIRE](#)].
- [4] A. Das, N. Okada and N. Papapietro, *Electroweak vacuum stability in classically conformal B-L extension of the Standard Model*, *Eur. Phys. J. C* **77** (2017) 122 [[arXiv:1509.01466](https://arxiv.org/abs/1509.01466)] [[INSPIRE](#)].

- [5] A. Das, S. Oda, N. Okada and D.S. Takahashi, *Classically conformal $U(1)'$ extended standard model, electroweak vacuum stability and LHC Run-2 bounds*, *Phys. Rev. D* **93** (2016) 115038 [[arXiv:1605.01157](#)] [[INSPIRE](#)].
- [6] C. Corianò, L. Delle Rose and C. Marzo, *Vacuum stability in $U(1)'$ extensions of the Standard Model with TeV scale right handed neutrinos*, *Phys. Lett. B* **738** (2014) 13 [[arXiv:1407.8539](#)] [[INSPIRE](#)].
- [7] C. Corianò, L. Delle Rose and C. Marzo, *Constraints on abelian extensions of the Standard Model from two-loop vacuum stability and $U(1)_{B-L}$* , *JHEP* **02** (2016) 135 [[arXiv:1510.02379](#)] [[INSPIRE](#)].
- [8] E. Accomando et al., *Z' , Higgses and heavy neutrinos in $U(1)'$ models: from the LHC to the GUT scale*, *JHEP* **07** (2016) 086 [[arXiv:1605.02910](#)] [[INSPIRE](#)].
- [9] E. Accomando et al., *Novel SM-like Higgs decay into displaced heavy neutrino pairs in $U(1)'$ models*, *JHEP* **04** (2017) 081 [[arXiv:1612.05977](#)] [[INSPIRE](#)].
- [10] E. Accomando et al., *Extra Higgs boson and Z' as portals to signatures of heavy neutrinos at the LHC*, *JHEP* **02** (2018) 109 [[arXiv:1708.03650](#)] [[INSPIRE](#)].
- [11] M. Klasen, F. Lyonnet and F.S. Queiroz, *NLO+NLL collider bounds, Dirac fermion and scalar dark matter in the $B-L$ model*, *Eur. Phys. J. C* **77** (2017) 348 [[arXiv:1607.06468](#)] [[INSPIRE](#)].
- [12] P. Ilten, Y. Soreq, M. Williams and W. Xue, *Serendipity in dark photon searches*, *JHEP* **06** (2018) 004 [[arXiv:1801.04847](#)] [[INSPIRE](#)].
- [13] M. Lindner, F.S. Queiroz, W. Rodejohann and X.-J. Xu, *Neutrino-electron scattering: general constraints on Z' and dark photon models*, *JHEP* **05** (2018) 098 [[arXiv:1803.00060](#)] [[INSPIRE](#)].
- [14] J. Bellm et al., *HERWIG 7.0/HERWIG++ 3.0 release note*, *Eur. Phys. J. C* **76** (2016) 196 [[arXiv:1512.01178](#)] [[INSPIRE](#)].
- [15] A. Buckley et al., *Rivet user manual*, *Comput. Phys. Commun.* **184** (2013) 2803 [[arXiv:1003.0694](#)] [[INSPIRE](#)].
- [16] G.M. Pruna, *Phenomenology of the minimal $B-L$ model: the Higgs sector at the Large Hadron Collider and future Linear Colliders*, Ph.D. thesis, Southampton University, Southampton, U.K. (2011), [[arXiv:1106.4691](#)] [[INSPIRE](#)].
- [17] F.F. Deppisch, P.S. Bhupal Dev and A. Pilaftsis, *Neutrinos and collider physics*, *New J. Phys.* **17** (2015) 075019 [[arXiv:1502.06541](#)] [[INSPIRE](#)].
- [18] T. Robens and T. Stefaniak, *Status of the Higgs singlet extension of the standard model after LHC Run 1*, *Eur. Phys. J. C* **75** (2015) 104 [[arXiv:1501.02234](#)] [[INSPIRE](#)].
- [19] J. Chakraborty, P. Konar and T. Mondal, *Constraining a class of $B-L$ extended models from vacuum stability and perturbativity*, *Phys. Rev. D* **89** (2014) 056014 [[arXiv:1308.1291](#)] [[INSPIRE](#)].
- [20] D. López-Val and T. Robens, *Δr and the W -boson mass in the singlet extension of the standard model*, *Phys. Rev. D* **90** (2014) 114018 [[arXiv:1406.1043](#)] [[INSPIRE](#)].
- [21] PARTICLE DATA GROUP collaboration, *Review of particle physics*, *Chin. Phys. C* **40** (2016) 100001 [[INSPIRE](#)].
- [22] CMS collaboration, *Search for heavy Majorana neutrinos in $\mu^\pm\mu^\pm + jets$ events in proton-proton collisions at $\sqrt{s} = 8$ TeV*, *Phys. Lett. B* **748** (2015) 144 [[arXiv:1501.05566](#)] [[INSPIRE](#)].

- [23] ATLAS collaboration, *Search for new high-mass phenomena in the dilepton final state using 36 fb^{-1} of proton-proton collision data at $\sqrt{s} = 13\text{ TeV}$ with the ATLAS detector*, *JHEP* **10** (2017) 182 [[arXiv:1707.02424](#)] [[INSPIRE](#)].
- [24] CMS collaboration, *Search for high-mass resonances in dilepton final states in proton-proton collisions at $\sqrt{s} = 13\text{ TeV}$* , *JHEP* **06** (2018) 120 [[arXiv:1803.06292](#)] [[INSPIRE](#)].
- [25] G. Cacciapaglia, C. Csáki, G. Marandella and A. Strumia, *The minimal set of electroweak precision parameters*, *Phys. Rev. D* **74** (2006) 033011 [[hep-ph/0604111](#)] [[INSPIRE](#)].
- [26] SLAC E158 collaboration, *Observation of parity nonconservation in Moller scattering*, *Phys. Rev. Lett.* **92** (2004) 181602 [[hep-ex/0312035](#)] [[INSPIRE](#)].
- [27] LEP, ALEPH, DELPHI, L3, OPAL, LEP ELECTROWEAK WORKING GROUP, SLD ELECTROWEAK GROUP, SLD HEAVY FLAVOR GROUP collaboration, *A combination of preliminary electroweak measurements and constraints on the standard model*, [hep-ex/0312023](#) [[INSPIRE](#)].
- [28] M. Carena, A. Daleo, B.A. Dobrescu and T.M.P. Tait, *Z' gauge bosons at the Tevatron*, *Phys. Rev. D* **70** (2004) 093009 [[hep-ph/0408098](#)] [[INSPIRE](#)].
- [29] CHARM-II collaboration, *Measurement of differential cross-sections for muon-neutrino electron scattering*, *Phys. Lett. B* **302** (1993) 351 [[INSPIRE](#)].
- [30] LHCb collaboration, *Search for dark photons produced in 13 TeV pp collisions*, *Phys. Rev. Lett.* **120** (2018) 061801 [[arXiv:1710.02867](#)] [[INSPIRE](#)].
- [31] CMS collaboration, *Properties of the Higgs-like boson in the decay $H \rightarrow ZZ \rightarrow 4l$ in pp collisions at $\sqrt{s} = 7$ and 8 TeV*, CMS-PAS-HIG-13-002 (2013).
- [32] CMS collaboration, *Precise determination of the mass of the Higgs boson and tests of compatibility of its couplings with the standard model predictions using proton collisions at 7 and 8 TeV*, *Eur. Phys. J. C* **75** (2015) 212 [[arXiv:1412.8662](#)] [[INSPIRE](#)].
- [33] S. Banerjee, M. Mitra and M. Spannowsky, *Searching for a heavy Higgs boson in a Higgs-portal B-L model*, *Phys. Rev. D* **92** (2015) 055013 [[arXiv:1506.06415](#)] [[INSPIRE](#)].
- [34] P.S. Bhupal Dev and A. Pilaftsis, *Light and superlight sterile neutrinos in the minimal radiative inverse seesaw model*, *Phys. Rev. D* **87** (2013) 053007 [[arXiv:1212.3808](#)] [[INSPIRE](#)].
- [35] PLANCK collaboration, *Planck 2015 results. XIII. Cosmological parameters*, *Astron. Astrophys.* **594** (2016) A13 [[arXiv:1502.01589](#)] [[INSPIRE](#)].
- [36] A. Alloul et al., *FeynRules 2.0 — A complete toolbox for tree-level phenomenology*, *Comput. Phys. Commun.* **185** (2014) 2250 [[arXiv:1310.1921](#)] [[INSPIRE](#)].
- [37] C. Degrande et al., *UFO — The Universal FeynRules Output*, *Comput. Phys. Commun.* **183** (2012) 1201 [[arXiv:1108.2040](#)] [[INSPIRE](#)].
- [38] G. Cowan, K. Cranmer, E. Gross and O. Vitells, *Asymptotic formulae for likelihood-based tests of new physics*, *Eur. Phys. J. C* **71** (2011) 1554 [*Erratum* *ibid.* **C 73** (2013) 2501] [[arXiv:1007.1727](#)] [[INSPIRE](#)].
- [39] A.L. Read, *Presentation of search results: the $CL(s)$ technique*, *J. Phys. G* **28** (2002) 2693 [[INSPIRE](#)].
- [40] B. Batell, M. Pospelov and B. Shuve, *Shedding light on neutrino masses with dark forces*, *JHEP* **08** (2016) 052 [[arXiv:1604.06099](#)] [[INSPIRE](#)].
- [41] ATLAS collaboration, *Measurement of the low-mass Drell-Yan differential cross section at $\sqrt{s} = 7\text{ TeV}$ using the ATLAS detector*, *JHEP* **06** (2014) 112 [[arXiv:1404.1212](#)] [[INSPIRE](#)].

- [42] ATLAS collaboration, *Measurement of the transverse momentum and ϕ_{η}^* distributions of Drell-Yan lepton pairs in proton-proton collisions at $\sqrt{s} = 8$ TeV with the ATLAS detector*, *Eur. Phys. J. C* **76** (2016) 291 [[arXiv:1512.02192](#)] [[INSPIRE](#)].
- [43] ATLAS collaboration, *Measurement of the double-differential high-mass Drell-Yan cross section in pp collisions at $\sqrt{s} = 8$ TeV with the ATLAS detector*, *JHEP* **08** (2016) 009 [[arXiv:1606.01736](#)] [[INSPIRE](#)].
- [44] ATLAS collaboration, *Search for triboson $W^{\pm}W^{\pm}W^{\mp}$ production in pp collisions at $\sqrt{s} = 8$ TeV with the ATLAS detector*, *Eur. Phys. J. C* **77** (2017) 141 [[arXiv:1610.05088](#)] [[INSPIRE](#)].
- [45] CMS collaboration, *Measurements of jet multiplicity and differential production cross sections of Z + jets events in proton-proton collisions at $\sqrt{s} = 7$ TeV*, *Phys. Rev. D* **91** (2015) 052008 [[arXiv:1408.3104](#)] [[INSPIRE](#)].
- [46] LHCb collaboration, *Measurement of the cross-section for $Z \rightarrow e^+e^-$ production in pp collisions at $\sqrt{s} = 7$ TeV*, *JHEP* **02** (2013) 106 [[arXiv:1212.4620](#)] [[INSPIRE](#)].
- [47] ATLAS collaboration, *$ZZ \rightarrow \ell^+\ell^-\ell'^+\ell'^-$ cross-section measurements and search for anomalous triple gauge couplings in 13 TeV pp collisions with the ATLAS detector*, *Phys. Rev. D* **97** (2018) 032005 [[arXiv:1709.07703](#)] [[INSPIRE](#)].
- [48] ATLAS collaboration, *Fiducial and differential cross sections of Higgs boson production measured in the four-lepton decay channel in pp collisions at $\sqrt{s} = 8$ TeV with the ATLAS detector*, *Phys. Lett. B* **738** (2014) 234 [[arXiv:1408.3226](#)] [[INSPIRE](#)].
- [49] ATLAS collaboration, *Measurement of ZZ production in pp collisions at $\sqrt{s} = 7$ TeV and limits on anomalous ZZZ and ZZ γ couplings with the ATLAS detector*, *JHEP* **03** (2013) 128 [[arXiv:1211.6096](#)] [[INSPIRE](#)].
- [50] ATLAS collaboration, *Measurements of Z γ and Z $\gamma\gamma$ production in pp collisions at $\sqrt{s} = 8$ TeV with the ATLAS detector*, *Phys. Rev. D* **93** (2016) 112002 [[arXiv:1604.05232](#)] [[INSPIRE](#)].
- [51] ATLAS collaboration, *Measurement of the electroweak production of dijets in association with a Z-boson and distributions sensitive to vector boson fusion in proton-proton collisions at $\sqrt{s} = 8$ TeV using the ATLAS detector*, *JHEP* **04** (2014) 031 [[arXiv:1401.7610](#)] [[INSPIRE](#)].
- [52] ATLAS collaboration, *Measurement of the k_t splitting scales in $Z \rightarrow \ell\ell$ events in pp collisions at $\sqrt{s} = 8$ TeV with the ATLAS detector*, *JHEP* **08** (2017) 026 [[arXiv:1704.01530](#)] [[INSPIRE](#)].
- [53] ATLAS collaboration, *Measurements of four-lepton production in pp collisions at $\sqrt{s} = 8$ TeV with the ATLAS detector*, *Phys. Lett. B* **753** (2016) 552 [[arXiv:1509.07844](#)] [[INSPIRE](#)].
- [54] ATLAS collaboration, *Measurement of total and differential W^+W^- production cross sections in proton-proton collisions at $\sqrt{s} = 8$ TeV with the ATLAS detector and limits on anomalous triple-gauge-boson couplings*, *JHEP* **09** (2016) 029 [[arXiv:1603.01702](#)] [[INSPIRE](#)].
- [55] CMS collaboration, *Measurements of the associated production of a Z boson and b jets in pp collisions at $\sqrt{s} = 8$ TeV*, *Eur. Phys. J. C* **77** (2017) 751 [[arXiv:1611.06507](#)] [[INSPIRE](#)].
- [56] LHCb collaboration, *Study of forward Z + jet production in pp collisions at $\sqrt{s} = 7$ TeV*, *JHEP* **01** (2014) 033 [[arXiv:1310.8197](#)] [[INSPIRE](#)].